Journal of Alloys and Compounds 520 (2012) 195–201

Contents lists available at SciVerse ScienceDirect

Journal of Alloys and Compounds

journal homepage: www.elsevier.com/locate/jallcom

# EPR properties of some new cadmium and rare-earth molybdates, molybdato-tungstates and their solid solutions

S.M. Kaczmarek[a,*], G. Leniec[a], H. Fuks[a], E. Tomaszewicz[b], G. Dąbrowska[b], T. Skibiński[a]

[a] Faculty of Mechanical Engineering and Mechatronics, Institute of Physics, West Pomeranian University of Technology, Al. Piastów 17, 70-310 Szczecin, Poland
[b] Department of Inorganic and Analytical Chemistry, West Pomeranian University of Technology, Al. Piastów 42, 71-065 Szczecin, Poland

ARTICLE INFO

*Article history:*
Received 21 October 2011
Received in revised form
30 December 2011
Accepted 3 January 2012
Available online 10 January 2012

*Keywords:*
Ceramics
Solid state reactions
Electron paramagnetic resonance
X-ray diffraction

ABSTRACT

A reactivity in the solid state between $CdMoO_4$ and $RE_2(MoO_4)_3$ or $RE_2(WO_4)_3$, where RE = Nd, Sm, Dy, was investigated using X-ray diffraction and electron paramagnetic resonance techniques. Obtained phases have shown scheelite-like structure, congruent melting and axial or close to axial symmetry of $RE^{3+}$ ions. The main type of magnetic interactions in samples under studies is proved to be ferromagnetic one. Besides $RE^{3+}$ ions, isolated and paired centers o molybdenum (5+) were found in the electron paramagnetic resonance spectra.



## 1. Introduction

It is known that molybdates and tungstates are a very important family of inorganic materials that have a high potential application in various fields, such as photoluminescence, microwave applications, optical fibers, scintillator and laser materials [1–12]. As phosphors, molybdates and tungstates have some advantages, e.g. a high thermal and chemical stability, a high average refractive index, a high X-ray absorption coefficient, a high light yield, a short decay time, and a low afterglow to luminescence. Solid state lasers based on molybdates or tungstates doped by rare-earth ions ($RE^{3+}$) show a very high stability of emission of nano- or femtoseconds pulses with a high peak power, high efficiency, long lifetime, and a low excitation threshold.

Known for several years, alkali rare-earth metal molybdates and tungstates ($ARE(XO_4)_2$, where $A^+$ = alkali metal ions, $RE^{3+}$ = rare earth ions, $X^{6+}$ = molybdenum or tungsten ions) are of particular interest since they are good laser hosts, an efficient Raman active medium, and have potential applications in quantum electronics, solid-state lighting and fluorescent labels [6,13–17]. Many of these compounds show the scheelite-type structure with the space group of $I4_1/a$. In this type structure, $A^+$ and $RE^{3+}$ ions exist in an environment of bisdisphenioid polyhedron build by eight oxygen ions, whereas, the molybdenum and tungsten ions are surrounded by four oxygen ions in a tetrahedral site. The similar ionic radii of tetrahedral coordinated of $Mo^{6+}$ (0.041 nm) and $W^{6+}$ (0.042 nm) ions may make it possible to prepare substitution solid solutions.

New scheelite-like $Cd_{0.25}Gd_{0.50}\square_{025}WO_4:Eu^{3+}$ solid solutions have been successfully synthesized for the first time by us using the conventional high-temperature solid-state method [18]. The photoluminescence investigations under ultraviolet–visible (UV) as well as under vacuum-ultraviolet–visible (VUV) excitation showed that these phases can generate a strong red emission and they are new promising red phosphors with potential applications for white-light-emitting diodes (WLEDs) [18]. Our earlier studies prompted us to search for new materials with interesting properties and promising applications. We also investigated the mutual reactivity in the solid state of cadmium molybdate ($CdMoO_4$, the scheelite-type structure) with some rare-earth metal molybdates of the formula $RE_2(MoO_4)_3$ or tungstates of the formula $RE_2(WO_4)_3$, where RE = Pr, Nd, Sm–Dy [19,20]. We synthesized new solid solutions: $Cd_{1-3x}RE_{2x}\square_xMoO_4$ and $Cd_{1-3x}RE_{2x}\square_x(MoO_4)_{1-3x}(WO_4)_{3x}$ (where the symbol □ means vacancies in a cation sublattice) for $0 < x \leq 0.25$, according to the following solid-state reactions [19,20]:

$$(1-3x)CdMoO_{4(s)} + xRE_2(MoO_4)_{3(s)} = Cd_{1-3x}RE_{2x}\square_xMoO_{4(s)} \quad (1)$$

$$(1-3x)CdMoO_{4(s)} + xRE_2(WO_4)_{3(s)} = Cd_{1-3x}RE_{2x}\square_x(MoO_4)_{1-3x}(WO_4)_{3x(s)} \quad (2)$$

The positions of the new solid solutions as well as the terminal phases: $Cd_{0.25}RE_{0.50}\square_{0.25}MoO_4$ and $Cd_{0.25}RE_{0.50}(MoO_4)_{0.25}\square_{0.25}(WO_4)_{0.75}$ are marked in the concentration tetrahedron of the

* Corresponding author. Tel.: +48 91 449 4585; fax: +48 91 449 4346.
*E-mail address:* skaczmarek@zut.edu.pl (S.M. Kaczmarek).

0925-8388/$ – see front matter © 2012 Elsevier B.V. All rights reserved.
doi:10.1016/j.jallcom.2012.01.010

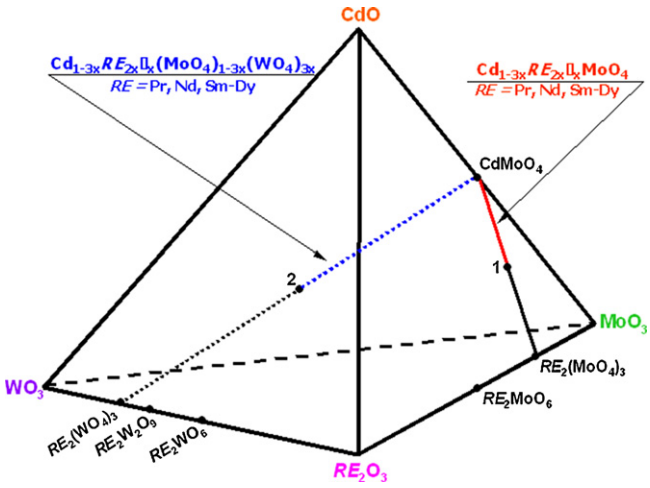


**Fig. 1.** Concentration tetrahedron of the $CdO–WO_3–RE_2O_3–MoO_3$ system: 1 – $Cd_{0.25}RE_{0.50}\square_{0.25}MoO_4$; 2 – $Cd_{0.25}RE_{0.50}\square_{0.25}(MoO_4)_{0.25}(WO_4)_{0.75}$.

$CdO–WO_3–RE_2O_3–MoO_3$ system, presented in Fig. 1. New cadmium and rare-earth metal molybdates and molybdato-tungstates form scheelite-type tetragonal lattice and they melt congruently [19,20]. Their lattice constants linearly decrease as increase an atomic number of $RE^{3+}$ ion [19,20]. According to the Vegard law, the unit cell parameters of new solid solutions also linearly decrease as the $CdMoO_4$ content in $CdMoO_4/RE_2(MoO_4)_3$ as well as in $CdMoO_4/RE_2(WO_4)_3$ initial reaction mixtures increases [19,20].

For the purpose of the present paper, we synthesized and analyzed by X-ray diffraction (XRD) and electron paramagnetic resonance (EPR) methods the following new phases: $Cd_{0.25}RE_{0.50}\square_{0.25}MoO_4$, $Cd_{0.25}RE_{0.50}\square_{0.25}(MoO_4)_{0.25}(WO_4)_{0.75}$ (RE = Nd and Dy) as well as some $Cd_{1-3x}RE_{2x}\square_xMoO_4$ and $Cd_{1-3x}RE_{2x}\square_x(MoO_4)_{1-3x}(WO_4)_{3x}$ solid solutions for RE = Nd and Dy and for different concentrations of a paramagnetic ion.

## 2. Materials and methods

The following metal oxides: CdO, $MoO_3$, $WO_3$, $Nd_2O_3$, $Sm_2O_3$ and $Dy_2O_3$ (all with the purity not less than 99.9%, Aldrich or Fluka) were used as starting materials. Cadmium molybdate and rare-earth metal molybdates and tungstates ($RE_2(MoO_4)_3$ and $RE_2(WO_4)_3$) were prepared by the solid state reactions described previously [19,20]. XRD method (X-ray diffractometer HZG-4, Cu Kα radiation, λ = 0.15418 nm) was used to an identification of prepared samples. XRD results showed that all of synthesized powders are monophased and they exhibit the scheelite-type structure. Fig. 2 shows XRD patterns of some obtained phases.

Powdered samples of $Cd_{0.9850}Nd_{0.0100}\square_{0.0050}MoO_4$ (composition of an initial mixture – 99.50 mol.% $CdMoO_4$ and 0.50 mol.% $Nd_2(MoO_4)_3$), $Cd_{0.9706}Sm_{0.0196}\square_{0.0098}MoO_4$ (99.00 mol.% $CdMoO_4$ and 1.00 mol.% $Sm_2(MoO_4)_3$), $Cd_{0.9850}Nd_{0.0100}\square_{0.0050}(MoO_4)_{0.9850}(WO_4)_{0.0150}$ (99.50 mol.% $CdMoO_4$ and 0.50 mol.% $Nd_2(WO_4)_3$) and $Cd_{0.9286}Nd_{0.0476}\square_{0.0238}(MoO_4)_{0.9286}(WO_4)_{0.0714}$ (97.50 mol.% $CdMoO_4$ and 2.50 mol.% $Nd_2(WO_4)_3$) as well as $Cd_{0.9850}Dy_{0.0100}\square_{0.0050}MoO_4$ (99.50 mol.% $CdMoO_4$ and 0.50 mol.% $Dy_2(MoO_4)_3$), $Cd_{0.9850}Dy_{0.0100}\square_{0.0050}(MoO_4)_{0.9850}(WO_4)_{0.0150}$ (99.50 mol.% $CdMoO_4$ and 0.50 mol.% $Dy_2(WO_4)_3$), $Cd_{0.25}Dy_{0.50}\square_{0.25}MoO_4$ (50.00 mol.% $CdMoO_4$ and 50.00 mol.% $Dy_2(MoO_4)_3$) and $Cd_{0.25}Dy_{0.50}\square_{0.25}(MoO_4)_{0.25}(WO_4)_{0.75}$ (50.00 mol.% $CdMoO_4$ and 50.00 mol.% $Dy_2(WO_4)_3$) have been investigated using the X-band EPR technique at temperatures of 7-295 K range using a conventional X-band Bruker ELEXSYS E 500 CW-spectrometer operating at 9.5 GHz with 100 kHz magnetic field modulation. The samples under measurements were in fine powder form. The first derivative of the powder absorption spectra has been recorded as a function of the applied magnetic field. Temperature dependence of the EPR spectra of the powdered sample was recorded using an Oxford Instruments ESP nitrogen-flow cryostat. The optimization of the spin-Hamiltonian parameters and EPR data simulation was achieved by using the software package SIMPOW [22,23] and EPR-NMR [23,24].

## 3. Results and discussion

Resonance spectra of all samples under studies are rather complex (Figs. 3 and 7–10), indicating on the existence of both: $RE^{3+}$ and reduced $Mo^{5+}$ or $W^{5+}$ magnetic species. The $RE^{3+}$ signal is observed only at temperatures below 30 K, whereas transition metal (Mo and W) (Cd, although transition metal, is not paramagnetic) signal is visible in whole temperature range.

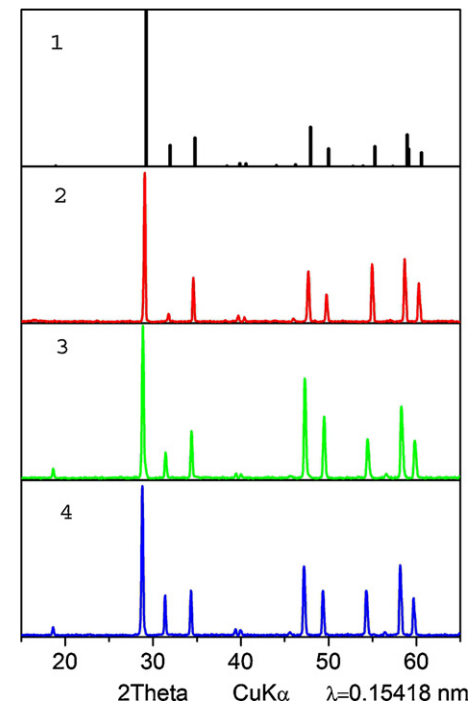


**Fig. 2.** XRD patterns: 1 – $CdMoO_4$ (the scheelite type structure, XRD pattern generated on the basis of [21]); 2 – $Cd_{0.9850}Dy_{0.0100}\square_{0.0050}(MoO_4)_{0.9850}(WO_4)_{0.0150}$; 3 – $Cd_{0.25}Dy_{0.50}\square_{0.25}MoO_4$; 4–$Cd_{0.25}Dy_{0.50}\square_{0.25}(MoO_4)_{0.25}(WO_4)_{0.75}$.

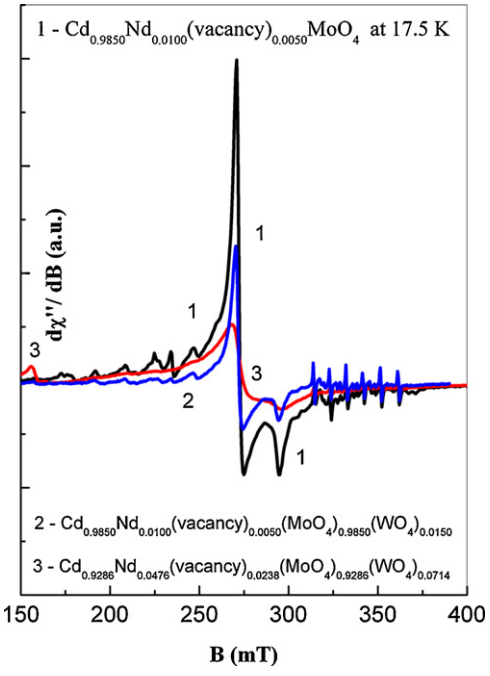


**Fig. 3.** EPR spectra of some of the samples under studies at ~17.5 K.

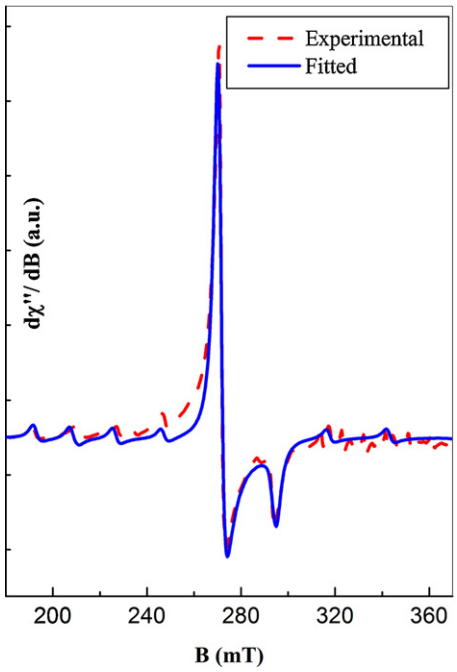


**Fig. 4.** EPR spectrum of $Cd_{0.9850}Nd_{0.0100}\square_{0.0050}(MoO_4)_{0.9850}(WO_4)_{0.0150}$ sample registered at 8 K and a result of SIMPOW program [20] fitting.

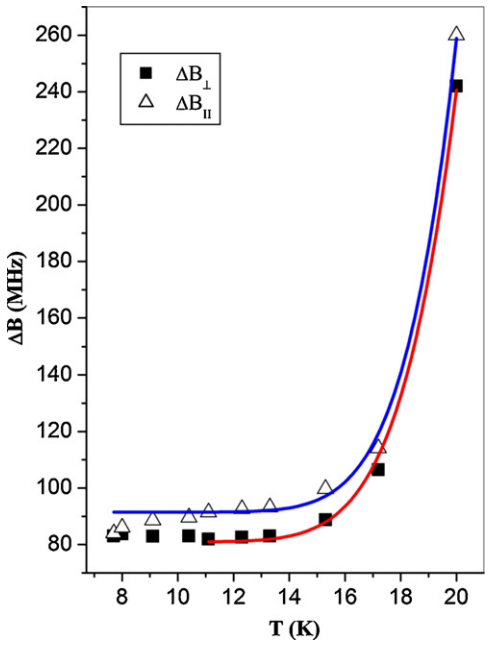


**Fig. 5.** Axial components of the linewidth vs. temperature for $Cd_{0.9850}Nd_{0.0100}\square_{0.0050}(MoO_4)_{0.9850}(WO_4)_{0.0150}$ sample and the result of fitting done by using Eq. (3).

### 3.1. EPR studies of $Cd_{1-3x}Nd_{2x}\square_xMoO_4$ and $Cd_{1-3x}Nd_{2x}\square_x(MoO_4)_{1-3x}(WO_4)_{3x}$ solid solutions

#### 3.1.1. Neodymium centers

Fig. 3 shows a low temperature EPR signal for three solid solutions containing neodymium ions: $Cd_{0.9850}Nd_{0.0100}\square_{0.0050}MoO_4$, $Cd_{0.9850}Nd_{0.0100}\square_{0.0050}(MoO_4)_{0.9850}(WO_4)_{0.0150}$ and $Cd_{0.9286}Nd_{0.0476}\square_{0.0238}(MoO_4)_{0.9286}(WO_4)_{0.0714}$. Main resonance signal, centered at magnetic field about 280 mT is connected with $Nd^{3+}$ paramagnetic species. As could be seen, for lower $Nd^{3+}$ content the resonance line is narrower and EPR signal is better resolved.

Being a Kramer's ion with high interval between a ground and excited states, $Nd^{3+}$ could be treated in double molybdatotungstates as a paramagnetic center with effective spin $S_{eff} = 1/2$. Spin Hamiltonian describing this case has the form:

$$H_s = \mu_B \mathbf{BgS} + \mathbf{SAI} \quad (3)$$

where first part of Eq. (3) represents the Zeeman term, and the second one describes hyperfine interaction between electronic and nuclear magnetic moment of odd neodymium isotopes ($Nd^{143}$ abundance 12%, $Nd^{145}$ abundance 8%, $I = 7/2$); $\mu_B$ – Bohr magneton, **B** – resonance magnetic field, **g** – spectroscopic tensor, **S** – spin operator, **A** – hyperfine interaction tensor, **I** – nuclear spin operator.

EPR signal of the $Nd^{3+}$ paramagnetic centers has been fitted by using SIMPOW procedure [22]. The result, shown in Fig. 4 is very satisfying and indicates on the axial or possible lower than axial a local crystal symmetry of neodymium ions. Perpendicular and parallel parts of ***g*** and ***A*** matrices have been clearly separated only for $Cd_{0.9850}Nd_{0.0100}\square_{0.0050}(MoO_4)_{0.9850}(WO_4)_{0.0150}$ sample, whereas for two other solid solutions only average values of ***A*** parameter were calculated. The results of the separation are collected in Table 1.

As could be concluded from Table 1, values of ***g*** and ***A*** parameters reveal only small changes, depending on the different value of local crystal field, concentration of $Nd^{3+}$ and type of transition metal ion. As we found, the temperature variation of the ***g*** and ***A*** parameters was insignificant.

All samples containing $Nd^{3+}$ revealed an interesting behavior of the linewidth as a function of a temperature. For example, in $Cd_{0.9850}Nd_{0.0100}\square_{0.0050}(MoO_4)_{0.9850}(WO_4)_{0.0150}$ solid solution, the width of the $Nd^{3+}$ line undergoes significant increase at temperatures above 10 K (Fig. 5), which suggests the presence of phonon, Raman and Orbach processes involved in spin–lattice relaxation phenomenon [23]. In this case share of excited states of $Nd^{3+}$ ions could be expressed by very well known the Orbach formula:

$$\Delta B = \Delta B_0 + Ce^{-W/kT} \quad (4)$$

where $\Delta B_0$ – residual linewidth, $C$ – experimental parameter, $W$ – energy interval between ground and first excited state, $k$ – Boltzmann constant.

The results of the simulation performed by using Eq. (4) are shown as solid lines in Fig. 5. The fitting is very well; calculated values of the $\Delta B_0$, $C$ and $W/k$ parameters for all three samples are collected in Table 2. In this table, we present additionally the Curie–Weiss (C–W) constant $\theta_{CW}$, expressing the strength of the magnetic interactions between $Nd^{3+}$ ions.

The values of a Curie–Weiss constant were calculated from the dependence of the integral intensity (EPR magnetic susceptibility) of the neodymium ions signal, $\chi_{EPR}$, on a temperature. In all cases, the $\chi_{EPR}(T)$ relation obeys the C–W law with some content of the Bleaney–Bowers (B–B) term (see also Eq. (7)), giving correction to

**Table 1**
Parameters of ***g*** and ***A*** principal values calculated from SIMPOW [22] procedure.

| Formula of a solid solution | $g_\perp$ | $g_\parallel$ | $A_\perp$ (MHz) | $A_\parallel$ (MHz) |
|---|---|---|---|---|
| $Cd_{0.9850}Nd_{0.0100}\square_{0.0050}MoO_4$ | 2.491 | 2.291 | 744 | |
| $Cd_{0.9850}Nd_{0.0100}\square_{0.0050}(MoO_4)_{0.9850}(WO_4)_{0.0150}$ | 2.497 | 2.294 | 744 | 729 |
| $Cd_{0.9286}Nd_{0.0476}\square_{0.0238}(MoO_4)_{0.9286}(WO_4)_{0.0714}$ | 2.504 | 2.265 | 730 | |

**Table 2**
Parameters of Eq. (3) calculated from the fitting procedure.

| Formula of a solid solution | $\Delta B_0$ (MHz) | $C$ (MHz) | $W/k$ (K) | $\theta_{CW}$ (K) |
|---|---|---|---|---|
| $Cd_{0.9850}Nd_{0.0100}\square_{0.0050}MoO_4$ | 58 | $1.22 \times 10^6$ | 176 | 1.9 (1.2) |
| $Cd_{0.9850}Nd_{0.0100}\square_{0.0050}(MoO_4)_{0.9850}(WO_4)_{0.0150}$ | | | | |
| ($\perp$) | 81 | $4.23 \times 10^6$ | 204 | |
| ($_{||}$) | 91 | $10 \times 10^6$ | 220 | 0.13 (−20) |
| $Cd_{0.9286}Nd_{0.0476}\square_{0.0238}(MoO_4)_{0.9286}(WO_4)_{0.0714}$ | 245 | $1.1 \times 10^4$ | 83 | 3.3 |

overall $\theta_{CW}$ value. These corrections are presented in Table 2 in brackets. Below about 10 K, the integral intensity of $Nd^{3+}$ signal shows direct agreement with the C–W law.

Analyzing values from Table 2 one can conclude that with increasing content of neodymium ions the relaxation processes are stronger and the width of the resonance line is significantly higher. Simultaneously, the distance to the excited states of $Nd^{3+}$ becomes shorter with smaller excitation energy, $W$. Higher neodymium ions content leads, also, to increase in a mutual ferromagnetic interaction between $Nd^{3+}$ ions (compare $\theta_{CW}$ value for $Cd_{0.9850}Nd_{0.0100}\square_{0.0050}(MoO_4)_{0.9850}(WO_4)_{0.0150}$ and $Cd_{0.9286}Nd_{0.0476}\square_{0.0238}(MoO_4)_{0.9286}(WO_4)_{0.0714}$) but the share of $Mo^{5+}$ ions is not excluded in this mechanism, as we observe significant difference of $\theta_{CW}$ value for $Cd_{0.9850}Nd_{0.0100}\square_{0.0050}MoO_4$ and $Cd_{0.9850}Nd_{0.0100}\square_{0.0050}(MoO_4)_{0.9850}(WO_4)_{0.0150}$ samples.

Additionally, the $Cd_{0.9706}Sm_{0.0196}\square_{0.0098}MoO_4$ sample has been investigated, which did not show any EPR signal from $Sm^{3+}$, only some weak one from $Mo^{5+}$ ions.

#### 3.1.2. Molybdenum centers

Second group of interesting resonance lines observed in Fig. 3 includes six narrow EPR lines located at magnetic field 310–360 mT. These lines, appearing in whole temperature range, are better observed above 20 K, where a signal of $Nd^{3+}$ is absent.

Comparing EPR spectra for all three samples we have seen that these extra lines are clearly observed in the EPR spectrum of $Cd_{0.9850}Nd_{0.0100}\square_{0.0050}MoO_4$, whereas in $Cd_{0.9850}Nd_{0.0100}\square_{0.0050}(MoO_4)_{0.9850}(WO_4)_{0.0150}$ are almost invisible. It may indicate that the above mentioned signals depend on molybdenum ions content, and due to this fact could be ascribed to the $Mo^{5+}$ complex magnetic system developed in the structure. The presence of the $Mn^{2+}$ in the samples under studies was excluded. This conclusion seems to be confirmed by EPR result of magnetically silent $RE^{3+}$ sample, i.e. $Cd_{0.9706}Sm_{0.0196}\square_{0.0098}MoO_4$ (Fig. 6), where only $Mo^{5+}$ signal is expected. The six narrow lines are ascribed to the hyperfine structure of $Mo^{5+}$ odd isotopes ($Mo^{95}$ abundance 15.9%, $Mo^{97}$ abundance 9.6%, $I = 5/2$).

According to the EPR spectra shown in Fig. 6, we evaluated an average hyperfine parameter $\boldsymbol{A}$ for $Mo^{5+}$ ions as being equal to $\boldsymbol{A} = 9.5$ mT (266 MHz) for all three samples, where split between the two molybdenum isotopes was not observed. This value is similar to reported earlier by us for other $RE^{3+}$ molybdates and molybdatotungstates [23].

As one can see from Fig. 6, besides six lines of $Mo^{5+}$ odd isotopes the extra lines are observed, at magnetic field below 250 mT. Supposing the simplest complex model, i.e. the existence of magnetic Mo-Mo pairs with $S = 1$, we have performed EPR-NMR simulation [24] employing the spin Hamiltonian of the form:

$$H_s = \mu_B \mathbf{BgS} + D\left[S_z^2 - \frac{1}{3}S(S+1)\right] + E(S_x^2 - S_y^2) \quad (5)$$

The best results we obtained for axial local symmetry with $\boldsymbol{g}$-factor and zero field splitting values as follow: $g_\perp = 4.0$, $g_{||} = 2.8$, $D = 312$ mT, $E = 0$. The result of the simulation, shown as a lower spectrum in Fig. 6, is not perfect but generally reflects the complex nature of these molybdenum magnetic centers.

### 3.2. EPR studies of $Cd_{1-3x}Dy_{2x}\square_xMoO_4$ and $Cd_{1-3x}Dy_{2x}\square_x(MoO_4)_{1-3x}(WO_4)_{3x}$ solid solutions

#### 3.2.1. Dysprosium centers

Group of dysprosium containing samples: $Cd_{0.9850}Dy_{0.0100}\square_{0.0050}MoO_4$, $Cd_{0.9850}Dy_{0.0100}\square_{0.0050}(MoO_4)_{0.9850}(WO_4)_{0.0150}$, $Cd_{0.25}Dy_{0.50}\square_{0.25}MoO_4$ and $Cd_{0.25}Dy_{0.5}\square_{0.25}(MoO_4)_{0.25}(WO_4)_{0.75}$ investigated by using the EPR technique revealed the existence of the wide, irregular resonance signal, observed at different applied magnetic fields. This signal, registered only at temperatures below 31 K, we attributed to the $Dy^{3+}$ paramagnetic centers.

Analysis of the $Dy^{3+}$ signal requires applying the spin Hamiltonian expressed by Eq. (3), as dysprosium ions are Kramer's type ions, too, and have odd isotopes $^{161}Dy$ and $^{163}Dy$ with natural abundance 18.9 and 24.9, and nuclear spin $I = 5/2$. The results of the fitting of spin Hamiltonian parameters of Eq. (3) by using the SIMPOW procedure [22], are collected in Table 3. The estimation of the $\boldsymbol{A}$ values seems to be rather roughly, since the EPR linewidth is huge and split between the above mentioned two dysprosium isotopes was not observed.

The integral intensity of the $Dy^{3+}$ paramagnetic centers, $\chi_{EPR}$, as a function of temperature is presented in Figs. 7–10. As could be concluded from the figures, the $\chi_{EPR}(T)$ dependencies do not follow purely the Curie–Weiss relation in any case. The discrepancy could have different reasons. The splitting between energy levels of $Dy^{3+}$ ions is weaker than for $Nd^{3+}$ ions, so there is possibility of upper level contribution to the ground state. Correction of the integral

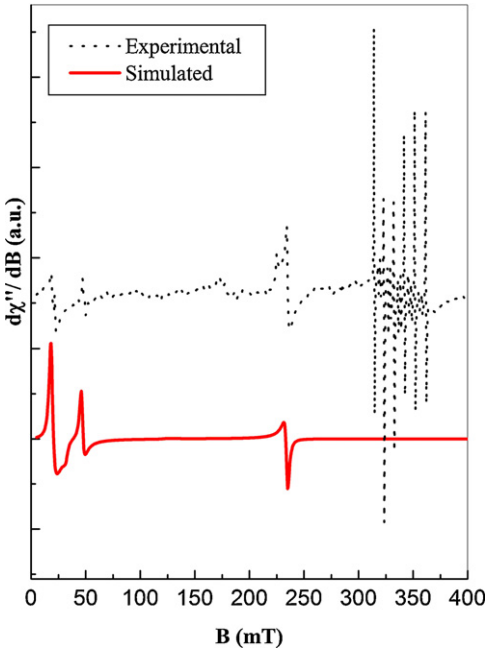


**Fig. 6.** EPR spectrum of the $Cd_{0.9706}Sm_{0.0196}\square_{0.0098}MoO_4$ sample at 32 K (upper spectrum) and the result of the EPR-NMR [24] simulation done by using Eq. (5) (lower spectrum).

**Table 3**
Spin Hamiltonian parameters of the $Dy^{3+}$ ions.

| No. | Formula of a solid solution | $g_\perp$ | $g_{\|\|}$ | $A_\perp$ (MHz) | $A_{\|\|}$ (MHz) |
|---|---|---|---|---|---|
| 1 | $Cd_{0.9850}Dy_{0.0100}\square_{0.0050}MoO_4$ | 1.76 | 6.39 | 2800 | 0 |
| 2 | $Cd_{0.9850}Nd_{0.0100}\square_{0.0050}(MoO_4)_{0.9850}(WO_4)_{0.0150}$ | 1.71 | 6.19 | 2800 | 0 |
| 3 | $Cd_{0.25}Dy_{0.50}\square_{0.25}MoO_4$ | 0.70 | 2.73 | 2800 | 0 |
| 4 | $Cd_{0.25}Dy_{0.50}\square_{0.25}(MoO_4)_{0.25}(WO_4)_{0.75}$ | 0.67 | 1.70 | 2800 | 0 |

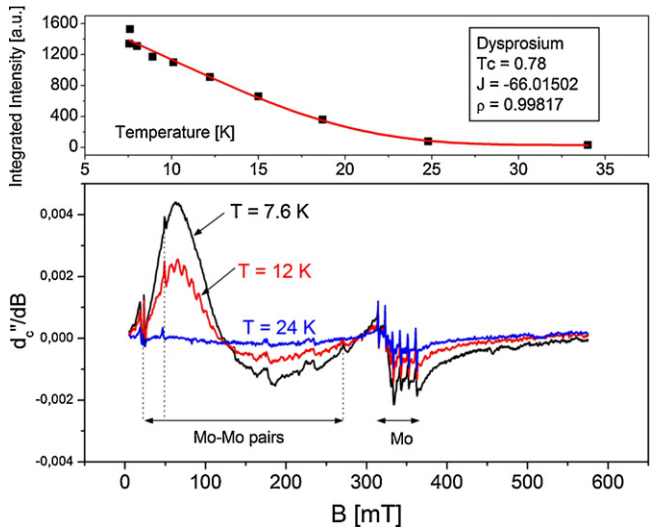


**Fig. 7.** Temperature dependence of the integrated intensity $\chi_{EPR}$, the solid line is the least square fitting of the intensity to the B–B–C function (Eq. (7)) with the fitting parameters presented in Table 4 (upper panel). Representative EPR spectra of the $Cd_{0.9850}Dy_{0.0100}\square_{0.0050}MoO_4$ solid solution registered at different temperatures (lower panel).

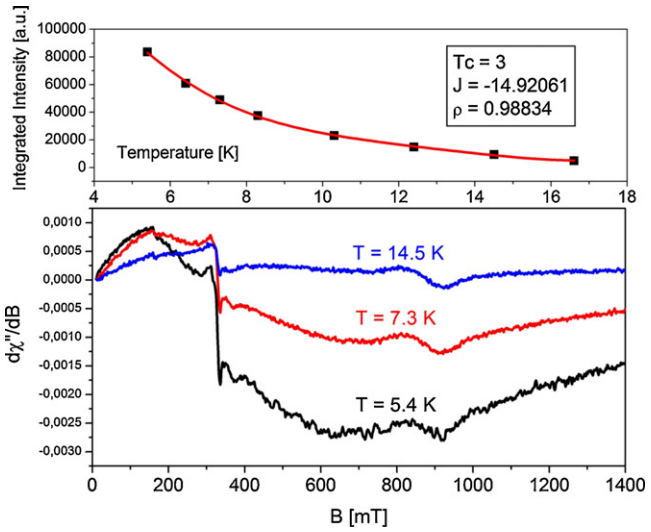


**Fig. 9.** Temperature dependence of the integrated intensity $\chi_{EPR}$, the solid line is the least square fitting to the B–B–C function (Eq. (7)) with the fitting parameters presented in Table 4 (upper panel). Representative EPR spectra of $Cd_{0.25}Dy_{0.50}\square_{0.25}MoO_4$ solid solution registered at different temperatures (lower panel).

intensity, $\Delta\chi_{EPR}$, arising from excited levels could be expressed in terms of the following equation:

$$\chi_{EPR}(T) = \frac{C_0}{T} \cdot \exp\left(-\frac{T_0}{T}\right) \quad (6)$$

where $T_0$ is the energy difference (expressed in K) between the ground state and the excited state. Curie–Weiss fittings at low temperatures were extended on higher temperatures for all of the solid solutions and the differences were calculated between experimental data and the fittings, $\Delta\chi_{EPR}$.

Another reason of the discrepancy observed for $\chi_{EPR}(T)$ relation could be connected with the existing of the complex (dimeric) magnetic centers of $Dy^{3+}$ ions. In that case the Eq. (7) should be employed (the Bleaney–Bowers–Curie equation, B–B–C). So, two

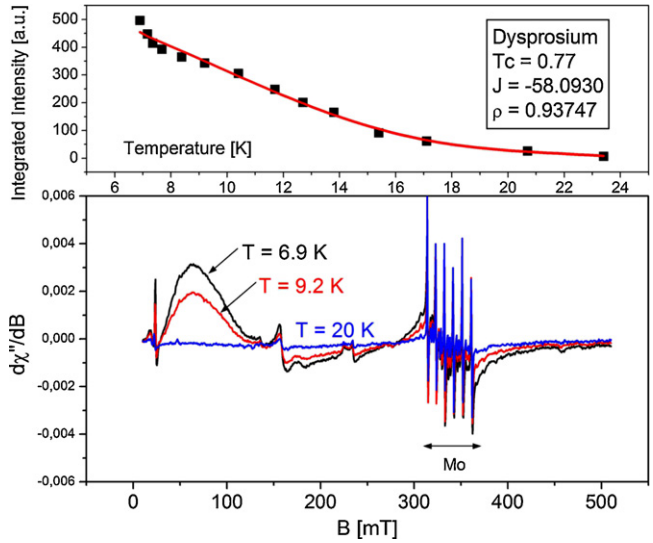


**Fig. 8.** Temperature dependence of the integrated intensity $\chi_{EPR}$, the solid line is the least square fitting to the B–B–C function (Eq. (7)) with the fitting parameters presented in Table 4 (upper panel). Representative EPR spectra of the $Cd_{0.9850}Dy_{0.0100}\square_{0.0050}(MoO_4)_{0.9850}(WO_4)_{0.0150}$ sample registered at different temperatures (lower panel).

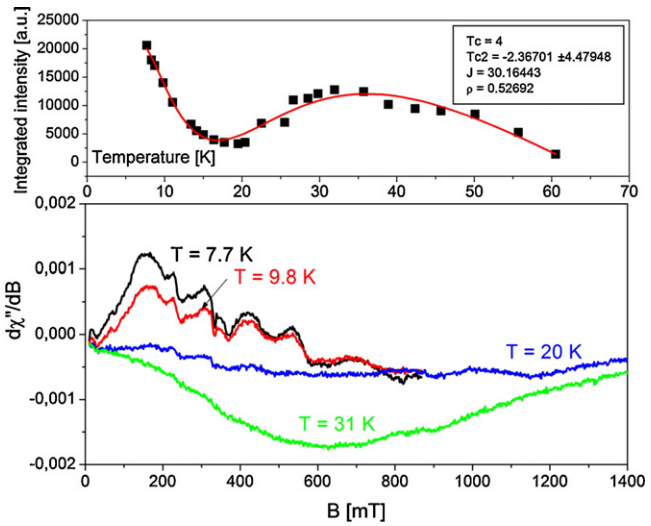


**Fig. 10.** Temperature dependence of the integrated intensity $\chi_{EPR}$, the solid line is the least square fitting to the B–B–C function (Eq. (7)) with the fitting parameters presented in Table 4 (upper panel). Representative EPR spectra of the $Cd_{0.25}Dy_{0.50}\square_{0.0050}(MoO_4)_{0.25}(WO_4)_{0.75}$ sample registered at different temperatures (lower panel).

**Table 4**
Fitting parameters of Eqs. (6) and (7).

| No. | Formula of a solid solution | $\rho$ | $J$ (K) | $\theta_{CW}$ (K) | $T_0$ (K) |
|---|---|---|---|---|---|
| 1 | $Cd_{0.9850}Dy_{0.0100}\square_{0.0050}MoO_4$ | 0.998 | −66.02 | 0.78 | 25 |
| 2 | $Cd_{0.9850}Nd_{0.0100}\square_{0.0050}(MoO_4)_{0.9850}(WO_4)_{0.0150}$ | 0.94 | −58.09 | 0.77 | 26.4 |
| 3 | $Cd_{0.25}Dy_{0.5}\square_{0.25}MoO_4$ | 0.988 | −14.92 | 3 | – |
| 4 | $Cd_{0.25}Dy_{0.5}\square_{0.25}(MoO_4)_{0.25}(WO_4)_{0.75}$ | 0.53 | 30.16 | 4/−2.37 | 16.34 |

possible correction mechanisms of $\chi_{EPR}(T)$ relation are taken into account. The results are presented in Table 4.

$$\chi_{EPR} = \frac{C_1}{T}\left[1 + \frac{1}{3}\exp\left(-\frac{2J}{kT}\right)\right]^{-1}(1-\rho) + \frac{C_2}{T-\theta_{CW}}\rho \quad (7)$$

where $k$ is Boltzmann constant, $C_1$, $C_2$ are constants, $T$ – temperature, $\theta_{CW}$ – Curie–Weiss temperature, $J$ – constant of exchange interactions and $\rho$ is the fraction of monomeric centers.

If analyze the above table one can find that the Curie–Weiss temperature for all of the solid solutions is positive and relatively small. It indicates on weak ferromagnetic interactions between dysprosium ions in low temperature ranges, i.e.: the solid solution No. 1 in the 7–15 K range, No. 2 in the 7–12 K range, No. 3 in the 5–8 K range and No. 4 in the 7–20 K range.

The fitting of the Eq. (6) to the experimental points shows that the excited state for the first two solid solutions (low dysprosium ions concentration) lays about ~25/26 K above the ground state; for the sample No. 3 we could not perform calculations due to too low amount of the experimental data, while for the sample No. 4 (higher dysprosium ions concentration) the excited state we found to be laying about 16 K above the ground state. It is possible that the splitting of the excited states of dysprosium ions depends on the $Dy^{3+}$ concentration.

From the fitting of the B–B–C function (Eq. (7)) it results that dimer contribution $(1-\rho)$ is low and magnetic interactions attributed to the dimers are weak. In the sample No. 1 it is only equal to 0.002%, No. 2–6%, and No. 3–1%. The sample No. 4 is an exception, showing weak ferromagnetic interactions at low temperatures ($T$ < 20 K), while at higher temperatures high contribution (47%) of magnetic entities reveal weak antiferromagnetic interactions ($T$ > 20). From Table 4 it results also that a value of the Curie–Weiss temperature is correlated with a moles number of $Dy^{3+}$ in the samples under studies. When it is lower (0.01), interactions between dysprosium ions are weaker and vice versa. Similar conclusion one can deduce in case of the values of Zeeman splitting (see Table 3). They correlate only with percentage content of $Dy^{3+}$ but not with the content of $MoO_4$ or $WO_4$ tetrahedra in structures of the solid solutions under investigations.

### 3.2.2. Molybdenum centers

The six narrow lines, similarly as in the case of the solid solutions doped by $Nd^{3+}$, are observed additionally in the EPR spectrum of low $Dy^{3+}$ doped samples (Figs. 7 and 8). They are also due to the hyperfine structure of $Mo^{5+}$ odd isotopes. According to the EPR spectra, we evaluated an average hyperfine parameter $\boldsymbol{A}$ for $Mo^{5+}$ ions as being equal to $\boldsymbol{A}$ = 9.6 mT for all samples, as in the case of $Nd^{3+}$ doped samples.

To analyze the magnetic interactions of molybdenum ions in the solid solutions under studies, we applied spin Hamiltonian of the form (3) for effective spin $S_{eff}$ = 1/2 and nuclear $I$ = 5/2. Values of the $\boldsymbol{g}$-factors are gathered in Table 3. The spin Hamiltonian parameters which we received are very close to described earlier for $Cd_{0.9706}Sm_{0.0196}\square_{0.0098}MoO_4$ solid solution. As one can see from Table 3, spin Hamiltonian parameters for isolated molybdenum ions are close each other. It indicates on stable surrounding of molybdenum ions ($MoO_4$). Small changes of the $\boldsymbol{g}$-factors are due to statistical positions of surrounding ions. Hyperfine splitting of the EPR lines due to molybdenum ions one can observe mainly for low doping with dysprosium ions.

We analyzed also the possibility of forming of molybdenum pairs applying spin Hamiltonian as described by Eq. (5). The presence of such kinds of entities is clearly seen in Figs. 7 and 8 for low $Dy^{3+}$ concentration (see additional lines at low magnetic fields). The simulation performed earlier for $Nd^{3+}$ doped samples fully reflects the shape of the additional lines.

## 4. Conclusions

New $Cd_{1-3x}RE_{2x}\square_xMoO_4$ and $Cd_{1-3x}RE_{2x}\square_x(MoO_4)_{1-3x}(WO_4)_{3x}$ solid solutions (where RE = Nd, Sm and Dy) were successfully prepared via the conventional solid-state reaction. As confirmed from the powder X-ray diffraction data, these molybdates and molybdato-tungstates crystallize in the tetragonal scheelite-type structure. Just as the known $Cd_{0.25}Gd_{0.50}\square_{025}WO_4$:$Eu^{3+}$ solid solutions, they are also excellent materials for many industrial applications (particularly, the solid solutions doped by $Nd^{3+}$ ions as solid-state lasers). The solid solutions under studies were also characterized by EPR technique. EPR signal of the $Nd^{3+}$ and $Dy^{3+}$ paramagnetic centers in the above solid solutions has been fitted by using the SIMPOW procedure. The results indicated on the axial or close to axial crystal symmetry of local surrounding of the paramagnetic ions. The values of a Curie–Weiss temperature were found to be positive and relatively small (below 3 K). So, the main type of magnetic interactions in these solutions is proved to be ferromagnetic one. Phases doped by $Nd^{3+}$ revealed phonon, Raman and Orbach processes involved in spin–lattice relaxation phenomenon, while $Dy^{3+}$ doped ones revealed the contribution of both: excited states and dimers in the integral intensity (EPR magnetic susceptibility) dependence on a temperature. From the fitting of the dependence to the B–B–C function it resulted that dimer contribution ($\rho$) was low and magnetic interactions of the dimers were generally weak. Besides $Nd^{3+}$ and $Dy^{3+}$ ions, uncontrolled magnetic entities were found in the EPR spectra of both kinds' doping as magnetically active. They were ascribed to $Mo^{5+}$ isolated ions and pairs.

## Acknowledgment

This work is supported by research grant No. N209 336937 (2009–2012) from the Polish Ministry of Science and High Education.

## References

[1] C. Feldmann, T. Jüstel, C.R. Ronda, P.J. Schmidt, Adv. Funct. Mater. 13 (2003) 511.
[2] A. Kato, S. Oishi, T. Shishido, M. Yamazaki, S. Iida, J. Phys. Chem. Solids 66 (2005) 2079.
[3] H. Li, H.K. Yang, B.K. Moon, B. Ch Choi, J.H. Jeong, K. Jang, H.S. Lee, S.S. Yi, J. Alloys Compd. 509 (2011) 8788.
[4] C. Tu, M. Qiu, J. Li, H. Liao, Opt. Mater. 16 (2001) 431.
[5] X. He, M. Guan, Ch Zhang, T. Shang, N. Lian, Y. Yao, J. Alloys Compd. 509 (2011) L341.
[6] Y. Jin, J. Zhang, Z. Hao, X. Zhang, X.-J. Wang, J. Alloys Compd. 509 (2011) L348.
[7] T. Kim, S. Kang, J. Lumin. 122-123 (2007) 964.
[8] K.G. Tshabalala, S.-H. Cho, J.-K. Park, Shreyas S. Pitale, I.M. Nagpure, R.E. Kroon, H.C. Swart, O.M. Ntwaeaborwa, J. Alloys Compd. 509 (2011) 10115.

[9] Y. Chen, H.K. Yang, S.W. Park, B.K. Moon, B.Ch. Choi, J.H. Jeong, K.H. Kim, J. Alloys Compd. 511 (2012) 123.
[10] Ch. Sun, F. Yang, T. Cao, Z. You, Y. Wang, J. Li, Z. Zhu, Ch Tu, J. Alloys Compd. 509 (2011) 6987.
[11] L. Nagornaya, G. Onyshchenko, E. Pirogov, N. Starzhinskiy, I. Tupitsyna, V. Ryzhikov, Yu Galich, Yu Vostretsov, S. Galkin, E. Voronkin, Nucl. Instrum. Methods Phys. Res. A (2005) 163.
[12] N. Klassen, S. Shmurak, B.S. Redkin, B. Ille, M. Lebeau, P. Lecoq, M. Schneegans, Nucl. Instrum. Methods Phys. Res. A 486 (2003) 431.
[13] A.A. Kaminskii, S.N. Bagaev, D. Grebe, J.J. Eichler, A.A. Pavlyuk, R. MacDonald, Quantum Electron. 26 (1996) 193.
[14] A.A. Kaminskii, H.J. Eichler, K. Ueda, N.V. Klassen, B.S. Redkin, L.E. Li, J. Findeisen, D. Jaque, J. García-Sole, J. Fernández, R. Balda, Appl. Opt. 38 (1999) 4533.
[15] Y.R. Do, Y.D. Huh, J. Electrochem. Soc. 147 (2000) 4385.
[16] C.H. Chiu, M.F. Wang, C.L. Lee, T.M. Chen, J. Solid State Chem. 180 (2007) 619.
[17] Ch. Guo, S. Wang, T. Chen, L. Luan, Y. Xu, Appl. Phys. A 94 (2009) 365.
[18] M. Guzik, E. Tomaszewicz, S.M. Kaczmarek, J. Cybińska, H. Fuks, J. Non-Cryst. Solids 356 (2010) 1902.
[19] E. Tomaszewicz, S.M. Kaczmarek, H. Fuks, Mater. Chem. Phys. 122 (2010) 595.
[20] E. Tomaszewicz, G. Dąbrowska, S.M. Kaczmarek, H. Fuks, J. Non-Cryst. Solids 356 (2010) 2059.
[21] M. Daturi, G. Busca, M.M. Borel, A. Leclaire, P. Piaggio, J. Phys. Chem. B 101 (1997) 4358.
[22] M. Nigels, Program SIMPOW, Illinois ESR Research Center NIH, IL, Division of Research Resources Grant No. RR0181, 2006.
[23] H. Fuks, S.M. Kaczmarek, G. Leniec, L. Macalik, B. Macalik, J. Hanuza, Opt. Mater. 32 (2010) 1560.
[24] M.J. Mombourquette, J.A. Weil, D.G. McGavin, EPR-NMR User's Manual, Department of Chemistry, University of Saskatchewan, Saskatoon, SK, Canada, 1999.